Effects of injected atomic coherence in broad-area lasers

Oscar G. Calderón,* Eduardo Cabrera, F. Carreño, M. A. Antón, Sonia Melle, and J. M. Guerra
Departamento de Optica, Universidad Complutense de Madrid, Ciudad Universitaria s/n, 28040 Madrid, Spain
(Received 25 May 2005; published 14 September 2005)

We analyze the effect of injected atomic coherence on transverse patterns of a broad area laser by means of the semiclassical two-level Maxwell-Bloch equations. A single longitudinal mode is considered. The injected atomic coherence forces a spatially homogeneous profile to appear and locks the field phase to a single value. Above a pump threshold value a very rich scenario of patterns is developed. Near threshold we find stationary patterns such as rhombic and hexagonal lattices. Well above threshold nonstationary patterns such as complex highly ordered vortex lattices traveling along the cross section, and nearly traveling waves appear.

DOI: 10.1103/PhysRevA.72.033811 PACS number(s): 42.65.Sf, 42.60.Jf, 42.50.Gy

I. INTRODUCTION

The formation and dynamics of transverse light patterns in broad area lasers and other nonlinear optical resonators have been a field of intense research in recent years [1–14] (see also special issue [15]). In these systems, the pattern formation is dominated by bulk parameters and nonlinearities of the active medium. It is customary, when transverse effects are included in the description of laser dynamics, to restrict the analysis to a single longitudinal mode approximation, thereby eliminating the additional complexity associated with longitudinal behavior [3]. It is well known that the pattern selected just above threshold depends on the sign of the cavity detuning Δ [1,2,8,16]. For negative detuning (cavities tuned above resonance) the laser selects a transverse spatially homogeneous solution, whereas for positive detuning (cavities tuned below resonance), a traveling wave (TW) is selected. In this last case, the laser emission is off-axis which helps the laser to emit on resonance. This phenomenon has been experimentally observed by Staliunas *et al.* [17] and by Hegarty *et al.* [18]. Other typical spatial structures that appear in lasers and laserlike systems (optical parametric oscillators and photorefractive oscillators) are the optical vortices which are localized structures characterized by the zero of the field amplitude, and the singularity of the field phase [1,19,20]. Vortices can arrange to form extended patterns (regular vortex lattices) [20–22].

Laser systems can be modified in order to show amplitude bistability response which corresponds to a change of the nature of the Hopf bifurcation from supercritical to subcritical. This phenomenon leads to the formation of bright localized structures or spatial solitons. Laser cavity solitons have been only shown to exist in the following situations; a passive element (a saturable absorber) is placed inside the resonator [23,24], in the presence of two-photon amplification [25], and in dense amplifying medium, i.e., when local-field effects are important [26]. These localized structures are of great interest due to their potential applicability to information processing [27,28]. In summary, a rich variety of extended patterns (tilted waves, vortex lattices) and localized structures (optical vortices, amplitude domains, spatial solitons) can be observed in laser and laserlike nonlinear optical systems.

Other scenario of pattern formation appears when the usual field phase invariance is broken, so then a pitchfork bifurcation governs the laser dynamics. For example, this happens when the active atoms are damped by a squeezed vacuum field. In this case, phase solitons have been predicted [29], which consist in ring profiles in the intensity pattern. Concerning the temporal features, the squeezed vacuum field leads to a phase-locked steady-state laser field [30,31]. One of the main attractive of this type of lasers is the reduction of noise in their output field [32]. A closely idea about the quantum-noise reduction in lasers consists of lasers with injected atomic coherence [33–35]. It is possible to reduce simultaneously the photon-number noise and phase noise in the laser when the active atoms are injected in a coherent superposition of states [36]. The temporal behavior of lasers with injected atomic coherence has been studied by Carty and Sargent III [37,38], Bergou *et al.* [39], and Ge *et al.* [40,41]. They found that the laser frequency is locked to the atomic line frequency. Laser oscillation below the usual laser threshold, and even in the absence of an inversion, was obtained. All of the research in laser dynamics with injected atomic coherence has been based on the plane-wave approximation, that is, ignoring transverse effects in the medium or in the field.

In this work, we study the spatiotemporal dynamics of broad area lasers with injected atomic coherence. We focus on the role played by the initial atomic coherence in the pattern formation. The injected atomic coherence increases the pump threshold to obtain transverse patterns. Below this threshold, a spatially homogenous state is forced by the initial atomic coherence, whereas above this threshold a very rich pattern formation takes place. We find stationary rhombic and hexagonal lattices, complex highly-ordered vortex lattices traveling along the cross section, and nearly traveling waves.

This system has several resemblances with the problem of a laser with an injected signal. The effect of a weak external signal in the laser transverse dynamics has been studied first by Mandel *et al.* [42], for a negative value of the detuning and by Longhi [43], for the positive detuning case. In this

*Electronic addrress: oscargc@opt.ucm.es; URL: http://www.ucm.es/info/laserlab

system, and for a positive value of the detuning, a forced mode due to the external field also appears together with one, two or three tilted waves. In the next section the differences and resemblances between this case and our study will be pointed out in more detail.

The paper is organized as follows. In Sec. II we present the two-level Maxwell-Bloch equations when the initial injected atomic coherence is considered. In Sec. III, we analyze the pattern forced by the injected atomic coherence and its linear stability. The numerical simulations are presented in Sec. IV. Finally, Sec. V provides brief conclusions.

II. LASER EQUATIONS

The starting point for our analysis are the Maxwell-Bloch equations for a broad area homogeneously broadened two-level laser with plane and parallel mirrors in the rotating wave, slowly varying amplitude, and single-longitudinal-mode approximations, and taking into account the injected atomic coherence. This system of equations was previously derived by Carty and Sargent III [37] without diffraction to study the temporal dynamics of this laser:

$$\frac{\partial E}{\partial \tau} = ia\Delta_{\perp}E + \sigma(P-E) + i\Delta E, \tag{1}$$

$$\frac{\partial P}{\partial \tau} = -P + R_{21} + ED, \tag{2}$$

$$\frac{\partial D}{\partial \tau} = -\gamma\left[D - R + \frac{1}{2}(E^{*}P + \text{c.c.})\right], \tag{3}$$

where E, P, and D are the dimensionless slowly varying envelopes of the electric field, the electric polarization, and the population inversion, respectively. $\gamma \equiv \gamma_{\parallel}/\gamma_{\perp}$ and $\sigma = \kappa/\gamma_{\perp}$ are the population inversion decay rate and the cavity losses, respectively, in units of the polarization decay rate ($\gamma_{\perp}$). $\Delta = (\omega_{21}-\omega_c)/\gamma_{\perp}$ is the usual rescaled detuning between the atomic line center and the cavity frequency. R represents the pumping parameter. Light diffraction is taken into account by means of the transverse Laplacian term in the field equation, and is measured by the diffraction coefficient $a = c^2/(2\omega_{21}\gamma_{\perp}b^2)$, where b is the spatial transverse size of the laser. $\Delta_{\perp} = \partial_x^2 + \partial_y^2$ is the transverse Laplacian where x and y are normalized with the spatial scale b. The time τ is normalized versus the polarization decay rate ($\tau = \gamma_{\perp}t$).

The pumping process to the two-level system introduces a population inversion R. Now, we continue by allowing the pumping to posses a nonvanishing atomic coherence. The time dependence of the injected atomic coherence is fixed by the Bohr frequency condition of the transition ($e^{-i\omega_{21}t}$), but its spatial distribution may be chosen arbitrarily [37]. Thus, if we want to phase match the injected atomic coherence to the propagating laser field we consider the same longitudinal dependence, thus, a running wave e^{ikz}, where k is the wave vector of the longitudinal cavity mode with frequency ω_c, then $k = \omega_c/c$. Finally we introduce R_{21} which is the dimensionless slowly varying amplitude of the injected atomic coherence.

Note that Eqs. (1)–(3) have been developed by considering as reference frequency the atomic line frequency ω_{21}. We assume in the rest of the work that R_{21} has a real and positive value since its phase dependence can be eliminated from the laser equations.

Now, let us comment about the value of the injected atomic coherence parameter R_{21}. The pumping contributions to the upper ($|a\rangle$) and lower ($|b\rangle$) lasing levels are proportional to $|c_a|^2$ and $|c_b|^2$, respectively, where c_a and c_b are the probability amplitudes of the upper and lower lasing levels, respectively. These pumping contributions are the usual ones in standard lasers. Therefore, the population inversion created by the pumping R is proportional to $R \propto |c_a|^2 - |c_b|^2$. As we said above, the pumping generates a nonvanishing atomic coherence R_{21} proportional to $R_{21} \propto 2\sqrt{\gamma}c_a c_b^{*}$ (with the same proportionallity constant as R). In these expressions we have considered the changes of variables made to develop the laser equations (1)–(3). Using these expressions we can estimate the value of the injected atomic coherence parameter $R_{21} \simeq 2\sqrt{\gamma}R|c_a|\sqrt{1-|c_a|^2}/(1-2|c_a|^2)$. Therefore, it is easy to achieve population inversion ($|c_a| > 0.5$) with an atomic coherence value of the same order of magnitude as R.

The system of equations (1)–(3) can be written as in the model used by Longhi to study the case of a laser with an injected signal making the following change of variables: $e = E$, $p = P - R_{21}$, and $n = R - D$ [43]. The new equations are similar to the ones used by Longhi, except for the appearance of a new term in the inversion equation $[1/2(e^{*}R_{21} + eR_{21})]$. This new term measures the coupling of the laser field with the injected atomic coherence. The analysis made by Longhi in Ref. [43], is based on the derivation of amplitude equations which is valid close to the instability point. This analysis reveals the presence of stable patterns formed by one, two, or three traveling waves for low values of the pump parameter and the external signal. For high pump values the single tilted wave which characterizes the standard laser is recovered, whereas high values of the injected field makes the system to emit on a homogeneous transverse solution (forced mode). In our study, we will handle with the whole system of equations (1)–(3) which allow us to study the laser dynamics well above the threshold. In our case, a high value of the injected atomic coherence will make the laser to emit also on the forced mode, while high values of the pump parameter will tend to restore the single TW over a nonzero background, i.e., over a spatially homogeneous field. Close to this last situation a pattern called nearly traveling wave appears which consists of a strong and a weak counterpropagating TWs over the forced mode. Furthermore, more complex patterns and bifurcations appear between these two extremes.

III. FORCED MODE

The laser equations (1)–(3) admit a spatially homogeneous stationary state forced by the atomic coherence R_{21} that acts as a driving force for the laser. This is the solution found in previous works in the plane-wave approximation [37,39]. This forced mode is $E(\tau,\vec{x}) = E_h$, $P(\tau,\vec{x}) = P_h$, and $D(\tau,\vec{x}) = D_h$, with

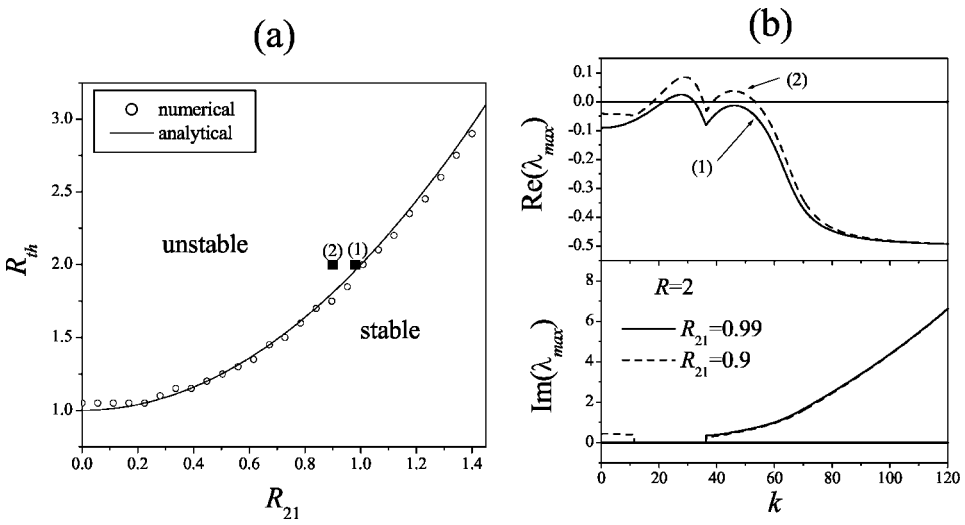

FIG. 1. (a) Neutral stability curve of the forced mode in the plane (R_{21},R). Both magnitudes are dimensionless. (b) The largest real part of any eigenvalue $\mathrm{Re}(\lambda_{\max})$ and its imaginary part $\mathrm{Im}(\lambda_{\max})$ as a function of the dimensionless wave vector k for $R=2$ and two values of the atomic coherence parameter: $R_{21}=0.99$ (solid line) corresponding to the point (1) in (a) and $R_{21}=0.9$ (dashed line) corresponding to the point (2) in (a). The rest of parameters are $\Delta=0.5$, $\sigma=0.5$, $\gamma=0.2$, and $a=5\times10^{-4}$.

$$P_h=\left(1-i\frac{\Delta}{\sigma}\right)E_h, \tag{4}$$

$$D_h=R-|E_h|^2, \tag{5}$$

$$R_{21}=E_h\left(1+|E_h|^2-R-i\frac{\Delta}{\sigma}\right). \tag{6}$$

From the last equation (6) we can obtain the intensity value $I_h\equiv|E_h|^2$ of the stationary spatially homogeneous state

$$I_h^3-2(R-1)I_h^2+\left[(R-1)^2+\frac{\Delta^2}{\sigma^2}\right]I_h-R_{21}^2=0. \tag{7}$$

This equation leads to three stationary solutions when the condition

$$(R-1)^2>3\frac{\Delta^2}{\sigma^2} \tag{8}$$

is fulfilled. Otherwise there is only one stationary solution. The phase of the stationary field $\phi_h[E_h=|E_h|\exp(i\phi_h)]$ is given by

$$\tan\phi_h=\frac{\Delta/\sigma}{1+I_h-R}, \tag{9}$$

where only one of the two possible solutions of Eq. (9)—differing by π—is valid, i.e., satisfies Eq. (6). Then, phase domains and phase solitons are not possible since the initial atomic coherence locks the field phase to a single value. This is in contrast to the laser with squeezed vacuum, where two different values of the locked-phase were obtained [29].

A. Linear stability analysis of the forced mode

We are going to study the stability of this homogeneous solution—forced by the initial atomic coherence—to finite sideband perturbations by linearizing about the spatially homogeneous stationary solution given by Eqs. (4)–(6). We follow the stability analysis performed by Jakobsen *et al.* [8] and Lega *et al.* [16]:

$$E=E_h+e_1e^{i\vec{k}\cdot\vec{x}}+e_2e^{-i\vec{k}\cdot\vec{x}},$$

$$P=P_h+p_1e^{i\vec{k}\cdot\vec{x}}+p_2e^{-i\vec{k}\cdot\vec{x}},$$

$$D=D_h+de^{i\vec{k}\cdot\vec{x}}+d^*e^{-i\vec{k}\cdot\vec{x}}, \tag{10}$$

where e_1, e_2, p_1, p_2, and d are the perturbations and $\vec{k}$ is the perturbation wave vector. Then we obtain $\partial_\tau\vec{v}=\mathcal{M}(\vec{k})\vec{v}$, where $\mathcal{M}$ is a 5×5 matrix and $\vec{v}$ denotes the column vector $(e_1,e_2^*,p_1,p_2^*,d)^T$. The time dependence of $\vec{v}$ is chosen as $e^{\lambda\tau}$, λ being the eigenvalues of $\mathcal{M}$. Then the homogeneous stationary solution is stable if, for all values of $\vec{k}$, the matrix of the coefficients $\mathcal{M}$ has all its eigenvalues with negative real part. If any eigenvalue has positive real part, the forced mode is unstable. The problem of finding the eigenvalues of the 5×5 matrix has been approached numerically. This analysis gives us information about the stability area of this stationary solution. Let us now to consider the following parameters: $\sigma=0.5$, $\gamma=0.2$, and $a=5\times10^{-4}$. In Fig. 1(a) we plot the stability diagram in the plane (R_{21},R) for a detuning $\Delta=0.5$ showing the stability region of the forced mode. The open circles are the neutral stability curve of the forced mode calculated numerically as explained above. In all the cases we have found that at the bifurcation point the most unstable wave has a wave vector close to 30 which corresponds to the usual excited wave in standard lasers, i.e., $k=\sqrt{\Delta/a}$. Concerning to the nature of the bifurcation we obtain that it is governed by a real eigenvalue which indicates that a pitchfork bifurcation is responsible of the dynamics. This result is in contrast to the usual laser where the bifurcation takes place through a complex eigenvalue, that is, by means of a Hopf bifurcation. For example, Fig. 1(b) shows the real part and the imaginary part of the maximum eigenvalue $\lambda_{\max}$ versus the perturbation wave number k for a pump value $R=2$ and two values of the atomic coherence parameter: $R_{21}=0.99$ (solid line) and $R_{21}=0.9$ (dashed line). The first curve [solid line in Fig. 1(b)] corresponds to a situation just above the instability point. Therefore, a TW with a wave vector close to the usual one $k\simeq\sqrt{\Delta/a}$ makes unstable the forced mode through a real eigenvalue, which agrees with our pre-

vious explanation. However, if we move further away from the instability point [see dashed line in Fig. 1(b)] two different instabilities take place. As well as the previous one, another TW with a larger wave vector grows. This last TW presents a complex eigenvalue which leads to a Hopf bifurcation. Therefore, in this regime, transverse patterns involving both type of instabilities and TWs are expected.

Now, let us go to try to obtain analytical expressions about the stability of the forced mode. The characteristic polynomial of the eigenvalue problem can be written as

$$[(1+\lambda)(\sigma+\lambda)-\sigma D_h]\left\{2(2\sigma+\lambda)|E_h|^2+\frac{2}{\gamma}(\gamma+\lambda)\times[(1+\lambda)(\sigma+\lambda)-\sigma D_h]\right\}$$
$$=(\Delta-ak^2)(1+\lambda)\left[2ak^2|E_h|^2-\frac{2}{\gamma}(\gamma+\lambda)(\Delta-ak^2)(1+\lambda)\right]. \quad (11)$$

As we have mentioned above, the wave that grows faster at the instability point has a wave vector of $k\simeq\sqrt{\Delta/a}$. If we take into account this result the right hand of the characteristic polynomial equation (11) becomes zero, and then we obtain a quadratic and a cubic equations. In other words, if we analyze the stability of the forced mode against a perturbation wave with wave vector $k=\sqrt{\Delta/a}$, the eigenvalue problem can be solved analytically. The quadratic equation yields the two eigenvalues

$$\lambda=-\frac{1+\sigma}{2}\pm\sqrt{\left(\frac{1+\sigma}{2}\right)^2+\sigma(D_h-1)}. \quad (12)$$

So, we can directly obtain the instability condition which reads $D_h\geqslant 1$. We can see that the bifurcation takes place through a real eigenvalue, in agreement with the numerical results. Now, we can calculate the threshold pump value (the neutral stability curve) from $D_h=1$, and we obtain

$$R_{\mathrm{th}}=1+\frac{\sigma^2}{\Delta^2}R_{21}^2, \quad (13)$$

so, if R is larger than the threshold value given by Eq. (13), the forced mode becomes unstable and then a pattern is expected. This threshold pump obtained analytically agrees with the one obtained numerically as is shown in Fig. 1(a). We clearly see from expression (13) that the pump threshold value to reach a pattern increases as R_{21} becomes larger. In the case of $R_{21}=0$, we recover the usual threshold value of 1. So, in principle, the injected atomic coherence tries to maintain an homogeneous state, i.e., the forced mode.

IV. NUMERICAL SIMULATIONS

We have numerically integrated Eqs. (1)–(3) in a square dibimensional lattice of 101×101 cells with periodic boundary conditions by means of a finite-difference algorithm. We have chosen a dimensionless cell size $\Delta x=0.01$ which allows a good representation of the traveling wave, that is, enough cells per wavelength and also enough number of phase rolls in the lattice. The system starts with small-amplitude random initial conditions and runs for times much larger than the characteristic relaxation times (final dimensionless time of the order of $\tau=5\times 10^4$ with a dimensionless time step $\Delta\tau=0.05$).

Let us analyze the spatiotemporal dynamics of the injected atomic coherence laser for a pump value below the usual threshold, i.e., $R<1$. We take $R=0.5$ and a detuning $\Delta=0.5$. We use the initial atomic coherence R_{21} as control parameter. Obviously, at $R_{21}=0$ (standard laser) there is not laser emission. For all of the values of R_{21} we obtain the spatially homogeneous stationary solution (4)–(6), in agreement with the linear stability analysis of Sec. III A, where we showed that the forced mode is always stable for pump values below 1 [see Fig. 1(a)].

Let us continue analyzing the pattern formation for a pump value above the usual threshold one, we take $R=2$. We also use the initial atomic coherence R_{21} as control parameter. First we consider a detuning equal to $\Delta=0.5$. As is well known, in the standard laser, i.e., $R_{21}=0$, we find a traveling wave (TW) with wave vector $k\simeq\sqrt{\Delta/a}$ (see first row in Fig. 2). However, a very rich scenario of patterns appears when an injected initial atomic coherence is considered. We have found several regimes depending on the value of R_{21}, as can be seen in Fig. 2 where we plot the intensity field (first column), the phase field (second column), and the power spectrum (third column) for different values of R_{21}. Note that a change of the initial atomic coherence means a change of the pump threshold [see Eq. (13)]. With the above parameter values and using the threshold condition given by Eq. (13), we obtain that the forced mode is stable for $R_{21}>(\Delta/\sigma)\sqrt{R-1}=1$. That is, there is a threshold value of R_{21} equal to 1 above which the forced mode appears (see last row in Fig. 2). Below the threshold value $R_{21}=1$, the homogeneous state loss its stability and a transverse pattern is expected. Close to threshold ($R/R_{\mathrm{th}}\simeq 1$), we obtain a stationary pattern which consists in two pairs of stationary waves with opposite wave vectors and a homogeneous state (see fifth row in Fig. 2). The two pairs of opposite waves are crossed at an angle of 55° and they have the same wave vector which corresponds to the usual one found in standard lasers, i.e., $k\simeq\sqrt{\Delta/a}$. This pattern corresponds to a rhombic lattice. However, stationary patterns formed by different number of stationary waves can be obtained by changing the cavity detuning. In particular, we find that the total number of stationary waves forming the stationary pattern increases with the value of the cavity detuning. In fact, a hexagonal lattice is found at $\Delta=1$ just above threshold ($R/R_{\mathrm{th}}\simeq 1$), as shown in Fig. 3. The lattice period agrees with the usual one given by $k\simeq\sqrt{\Delta/a}$. So, these stationary waves seem to be the basic mechanism of this hexagonal pattern. Hexagonal patterns have been previously found in lasers by means of spatial perturbations [44,45]. The simplest configuration of this type of stationary patterns that we obtain consists in two opposite stationary waves and the homogeneous state. This roll pattern is obtained at $\Delta=0.2$. We investigate in more detail this last pattern. We search for a solution of Eqs. (1)–(3) of the following form:

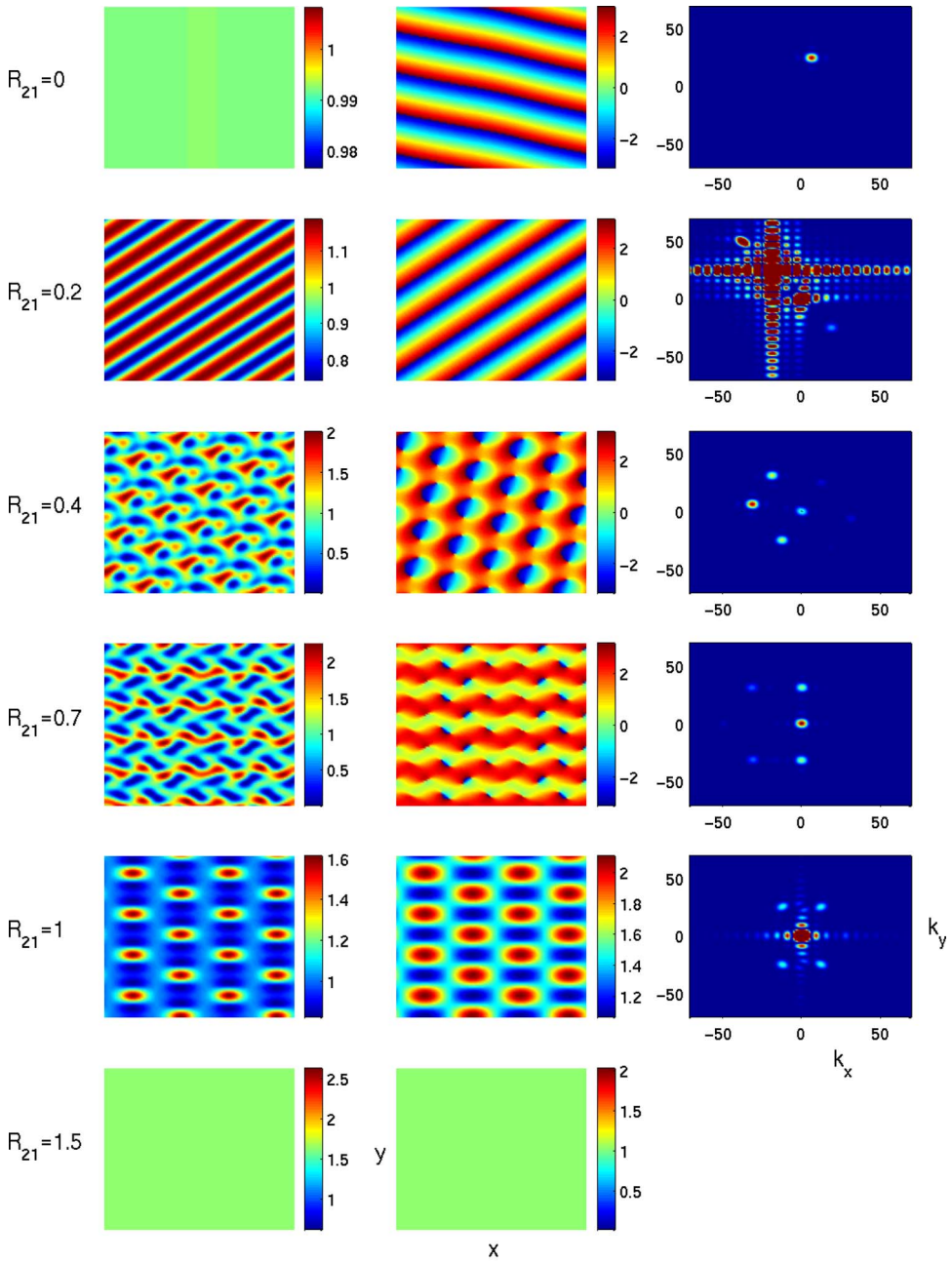

FIG. 2. (Color online.) The intensity field (first column), the phase field (second column), and the power spectrum (third column) for $\Delta=0.5$, $R=2$, and different values of the injected atomic coherence strength: $R_{21}=0$ (first row), $R_{21}=0.2$ (second row), $R_{21}=0.4$ (third row), $R_{21}=0.7$ (fourth row), $R_{21}=1$ (fifth row), and $R_{21}=1.5$ (sixth row). The rest of parameters are the same as in Fig. 1. All the magnitudes presented in this figure are dimensionless [including the real (x,y) and the Fourier (k_x,k_y) space coordinates].

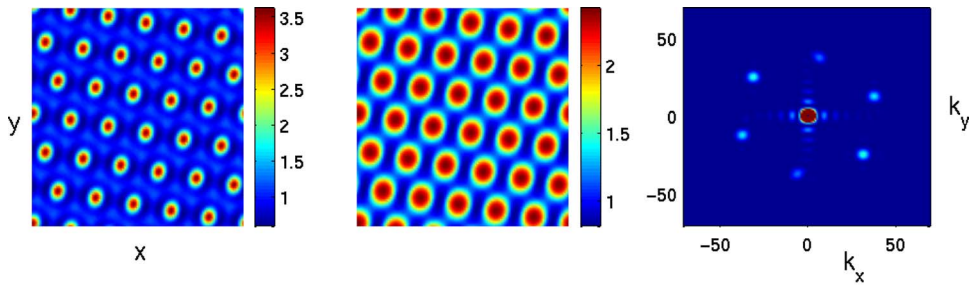

FIG. 3. (Color online.) The intensity field (first column), the phase field (second column), and the power spectrum (third column) for $\Delta=1$, $R=2$, and $R_{21}=2$. The rest of parameters are the same as in Fig. 1. All the magnitudes presented in this figure are dimensionless [including the real (x,y) and the Fourier (k_x,k_y) space coordinates].

$$E = E_0 + E_+ e^{i\vec{k}\cdot\vec{x}} + E_- e^{-i\vec{k}\cdot\vec{x}},$$

$$P = P_0 + P_+ e^{i\vec{k}\cdot\vec{x}} + P_- e^{-i\vec{k}\cdot\vec{x}},$$

$$D = D_0 + D_+ e^{2i\vec{k}\cdot\vec{x}} + D_+^* e^{-2i\vec{k}\cdot\vec{x}}. \quad (14)$$

Inserting Eqs. (14) into Eqs. (1)–(3) and neglecting the higher harmonics, we obtain that the homogeneous contribution is very similar to the forced mode

$$D_0 = (R + 2 - |E_0|^2)/3,$$

$$3R_{21} = E_0\left(1 + |E_0|^2 - R - i3\frac{\Delta}{\sigma}\right). \quad (15)$$

So the intensity I_0 and the phase field $\phi_0[E_0 \equiv \sqrt{I_0}\exp(i\phi_0)]$ satisfy the same equations of the forced mode by changing R_{21} and Δ/σ in Eqs. (7) and (9) by $3R_{21}$ and $3\Delta/\sigma$, respectively. Concerning to the stationary waves, we find that the wave vector is equal to $k^2=\Delta/a$. We also obtain that their amplitudes are equal to $|E_+|=|E_+|=\sqrt{D_0-1}$ and the phases obey the relation $[E_\pm=|E_\pm|\exp(i\phi_\pm)]$

$$\tan(\phi_+ + \phi_- - 2\phi_0) = \frac{4(\Delta/\sigma)}{(\Delta/\sigma)^2 - 4}. \quad (16)$$

These stationary patterns that appear just above threshold can be explained by means of a pitchfork bifurcation in agreement with the stability analysis shown in Fig. 1(b) (solid line).

More complex regimes appear when we move away from the threshold condition [Eq. (13)]. At $R_{21}=0.4$, i.e., $R/R_{\text{th}} \simeq 1.7$ (third row in Fig. 2) and $R_{21}=0.7$. i.e., $R/R_{\text{th}} \simeq 1.3$ (fourth row in Fig. 2), the pattern consists in a complex highly ordered vortex lattice. The zeros of the intensity field are accompanied by dislocation defects in the phase structure. Furthermore, the pattern is traveling along the cross section. This pattern resembles to the nonstationary vortex lattices found in class B lasers [46]. It is well known that when periodic boundaries are used, the vortex lattice can undergoes a parallel translation, as we obtain in our numerical results. We can observe in the intensity pattern corresponding to $R_{21}=0.4$ (see third row in Fig. 2) that there are two different shapes of vortices. They correspond to opposite topological charge optical vortices. As we have seen in Sec. III A, in this regime the stability analysis of the forced mode gives two different instabilities at different wave vectors. A pitchfork bifurcation—real eigenvalue—with a wave vector close to the usual one ($k \simeq \sqrt{\Delta/a}$), and a Hopf bifurcation—complex eigenvalue—with a TW with larger wave vector govern the transverse dynamics of the laser with injected atomic coherence. This situation corresponds to the dashed line in Fig. 1(b).

Finally, for very small values of the initial atomic coherence, $R_{21}=0.2$ which means pump values well above threshold $R/R_{\text{th}} \simeq 1.9$ (see second row in Fig. 2), a pattern dominated by a traveling wave (TW) and the homogeneous state appears. There is also a weak TW propagating in the opposite direction than the first one. The linear stability analysis of the homogeneous stationary state (see Sec. III A) for this region shows that the forced mode becomes unstable and the perturbation k that grows faster agrees with the wave vector found in the simulations. If we continue decreasing the initial atomic coherence strength the weak TW disappears, as happens for $R_{21}=0.1$, i.e., $R/R_{\text{th}} \simeq 2$. Therefore, the single tilted wave that characterizes the standard laser is recovered, although this TW is developed over a nonzero background field.

V. CONCLUSIONS

In this work we have studied the effect of injected atomic coherence in the spatiotemporal dynamics of a broad area laser. The temporal dynamics of lasers with injected atomic coherence has been previously studied in the plane-wave approximation, i.e., ignoring transverse effects in the medium or in the field [37–41]. Here we find that the injected atomic coherence forces a spatially homogeneous profile to appear and locks the field phase to a single value. So, the usual field phase invariance is broken, and a pitchfork bifurcation governs the pattern formation. Above a pump threshold value complex patterns appear. Close to threshold, we obtain stationary patterns such as rhombic lattices and hexagonal lattices. More complex regimes appear when we move away from the pump threshold. The pattern consists in a complex highly ordered vortex lattice traveling along the cross section. Finally, for very small values of the initial atomic coherence, a pattern dominated by a nearly traveling wave—a strong and a weak counterpropagating TWs—and the homogeneous state appears.

To conclude, let us discuss about the feasibility of the experimental realization of this laser system. First, the typical scheme of lasers with atomic coherence considers two excited atomic levels pumped at different rates and decaying to other levels, with negligible decay from upper to lower level [37]. This can be done using three-level atoms in which the two upper levels are the lasing transition. Therefore, the atoms are regularly injected into the laser cavity in a coherent superposition of the two upper levels and interact with the cavity laser field. This interaction is time limited by the decay of the two upper levels to the inert ground state. On the other hand, the atomic coherence is created through coherent transient phenomena which allows any desired superposition of the two lasing levels by controlling the interaction time of the atomic medium with an external short-time radiation field. Another difficulty that makes this physical problem a great challenge from the experimental point of view is the phase matching between the injected atomic coherence and laser field in both time and space. In Ref. [37] Carty and Sargent discuss this problem in depth. Agarwal *et al.* [35] suggest another scheme which is perhaps the simplest one from the point of view of experimental feasibility. They consider the active atoms being pumped into the upper level by the usual incoherent pump mechanism. In addition, these active atoms interact with an external field which is injected into the laser cavity from the side. This external field gives rise to the atomic coherence. Using the previous ideas we are going to consider the following experimental situation. We assume the laser medium as a two level system

inside a microresonator. This system will be pumped by a coherent pulsed laser field. If the pumping pulse width is of the order of the Rabi period, the system becomes coherently inverted. To have a quasistationary transverse pattern, the build-up time of the laser field must be much shorter than the coherence lifetime. A high-Q microresonator makes it more feasible to obtain a high Fresnel number and a short build-up time. In order to have an atomic coherence lifetime as large as possible it will be necessary to strongly cool the laser medium. A colinear pumping makes possible the phase matching between the injected coherence and laser field in both time and space.

ACKNOWLEDGMENTS

This work was supported by Project No. BFM2003-06292 (Spain) and by Project No. FIS2004-03267 (Spain).

[1] P. Coullet, L. Gil, and F. Rocca, Opt. Commun. **73**, 403 (1989).
[2] P. K. Jakobsen, J. V. Moloney, A. C. Newell, and R. Indik, Phys. Rev. A **45**, 8129 (1992).
[3] A. C. Newell and J. V. Moloney, *Nonlinear Optics* (Addison Wesley Publishing, Redwood City, California, 1992).
[4] E. J. D'Angelo, E. Izaquirre, G. B. Mindlin, G. Huyet, L. Gil, and J. R. Tredicce, Phys. Rev. Lett. **68**, 3702 (1992).
[5] F. T. Arecchi, S. Boccaletti, P. L. Ramazza, and S. Residori, Phys. Rev. Lett. **70**, 2277 (1993).
[6] Q. Feng, J. V. Moloney, and A. C. Newell, Phys. Rev. Lett. **71**, 1705 (1993).
[7] F. Prati, M. Brambilla, and L. A. Lugiato, Riv. Nuovo Cimento **17**, 1 (1994).
[8] P. K. Jakobsen, J. Lega, Q. Feng, M. Staley, J. V. Moloney, and A. C. Newell, Phys. Rev. A **49**, 4189 (1994).
[9] G. Huyet, M. C. Martinoni, J. R. Tredicce, and S. Rica, Phys. Rev. Lett. **75**, 4027 (1995).
[10] V. M. Pérez-García, I. Pastor, and J. M. Guerra, Phys. Rev. A **52**, 2392 (1995).
[11] R. Herrero, E. Grosse Westhoff, A. Aumann, T. Ackemann, Y. A. Logvin, and W. Lange, Phys. Rev. Lett. **82**, 4627 (1999).
[12] F. Encinas-Sanz, I. Leyva, and J. M. Guerra, Phys. Rev. Lett. **84**, 883 (2000).
[13] R. S. Bennink, V. Wong, A. M. Marino, D. L. Aronstein, R. W. Boyd, C. R. Stroud, S. Lukishova, and D. J. Gauthier, Phys. Rev. Lett. **88**, 113901 (2002).
[14] F. Encinas-Sanz, S. Melle, and O. G. Calderón, Phys. Rev. Lett. **93**, 213904 (2004).
[15] Special issue in pattern formation in lasers and other optical systems: Chaos, Solitons Fractals 10, n. 4–5 (1999).
[16] J. Lega, P. K. Jakobsen, J. V. Moloney, and A. C. Newell, Phys. Rev. A **49**, 4201 (1994).
[17] K. Staliunas, G. Slekys, and C. O. Weiss, Phys. Rev. Lett. **79**, 2658 (1997).
[18] S. P. Hegarty, G. Huyet, J. G. McInerney, and K. D. Choquette, Phys. Rev. Lett. **82**, 1434 (1999).
[19] C. Tamm, Phys. Rev. A **38**, 5960 (1988).
[20] M. Brambilla, F. Battipede, L. A. Lugiato, V. Penna, F. Prati, C. Tamm, and C. O. Weiss, Phys. Rev. A **43**, 5090 (1991).
[21] K. Staliunas and C. O. Weiss, Physica D **81**, 79 (1995).
[22] D. Hennequin, L. Dambly, D. Dangoise, and P. Glorieux, J. Opt. Soc. Am. B **11**, 676 (1994).
[23] N. N. Rosanov, J. Opt. Soc. Am. B **7**, 1057 (1990).
[24] V. B. Taranenko, K. Staliunas, and C. O. Weiss, Phys. Rev. A **56**, 1582 (1997).
[25] R. Vilaseca, M. C. Torrent, J. García-Ojalvo, M. Brambilla, and M. San Miguel, Phys. Rev. Lett. **87**, 083902 (2001).
[26] V. Ahufinger, J. García-Ojalvo, J. Mompart, M. C. Torrent, R. Corbalán, and R. Vilaseca, Phys. Rev. Lett. **91**, 083901 (2003).
[27] V. B. Taranenko and C. O. Weiss, IEEE J. Sel. Top. Quantum Electron. **8**, 488 (2002).
[28] S. Barland J. R. Tredicce, M. Brambilla, L. A. Ligiato, S. Balle, M. Guidici, T. Maggipento, L. Spinelli, G. Tissoni, T. Knödl, M. Miller, and R. Jäger, Nature (London) **419**, 699 (2002).
[29] O. G. Calderón, E. Cabrera, M. A. Antón, I. Gonzalo, F. Carreno, and J. M. Guerra, Phys. Rev. Lett. **92**, 163901 (2004).
[30] M. A. M. Marte and D. F. Walls, Phys. Rev. A **37**, 1235 (1988).
[31] M. A. Marte, H. Ritsch, and D. F. Walls, Phys. Rev. Lett. **61**, 1093 (1988).
[32] J. Gea-Banacloche, Phys. Rev. Lett. **59**, 543 (1987).
[33] C. Benkert, M. O. Scully, J. Bergou, and M. Orszag, Phys. Rev. A **41**, 4062 (1990).
[34] C. Benkert, M. O. Scully, and M. Orszag, Phys. Rev. A **42**, 1487 (1990).
[35] G. S. Agarwal, J. A. Bergou, C. Benkert, and M. O. Scully, Phys. Rev. A **43**, R6451 (1991).
[36] N. Lu and J. A. Bergou, Phys. Rev. A **40**, 237 (1989).
[37] T. Carty and Murray Sargent III, Phys. Rev. A **42**, 1544 (1990); **42**, 1532 (1990).
[38] T. Carty and M. Sargent III, Opt. Lett. **15**, 57 (1990).
[39] J. Bergou, J. Zhang, and A. Hourri, Phys. Rev. A **50**, 4188 (1994).
[40] G. Q. Ge, Y. Wu, X. Luo, and Z. Li, Phys. Rev. A **52**, 1783 (1995).
[41] G. Q. Ge, X. Luo, Y. Wu, and Z. Li, Phys. Rev. A **54**, 1604 (1996).
[42] P. Mandel, M. Georgiou, and T. Erneux, Phys. Rev. A **47**, 4277 (1993).
[43] S. Longhi, Phys. Rev. A **56**, 1553 (1997); **56**, 2397 (1997).
[44] M. Ciofini, A. Labate, R. Meucci, and P.-Y. Wang, Opt. Commun. **154**, 307 (1998).
[45] R. Meucci, A. Labate, M. Ciofini, and P.-Y. Wang, Quantum Semiclassic. Opt. **10**, 803 (1998).
[46] K. Staliunas and C. O. Weiss, J. Opt. Soc. Am. B **12**, 1142 (1995).